OPTICA

Automatic mitigation of dynamic atmospheric turbulence using optical phase conjugation for coherent free-space optical communications

Huibin Zhou,[1,*] Xinzhou Su,[1] Yuxiang Duan,[1] Yue Zuo,[1] Zile Jiang,[1] Muralekrishnan Ramakrishnan,[1] Jan Tepper,[2] Volker Ziegler,[2] Robert W. Boyd,[3] Moshe Tur,[4] and Alan E. Willner[1,5]

[1]Department of Electrical and Computer Engineering, University of Southern California, Los Angeles, California 90089, USA
[2]Central Research and Technology, Airbus, Taufkirchen, Germany
[3]Institute of Optics, University of Rochester, Rochester, New York 14627, USA
[4]School of Electrical Engineering, Tel Aviv University, Ramat Aviv 69978, Israel
[5]willner@usc.edu
*huibinzh@usc.edu

Received 10 September 2024; revised 21 December 2024; accepted 10 January 2025; published 31 January 2025

Coherent detection can provide enhanced receiver sensitivity and spectral efficiency in free-space optical (FSO) communications. However, turbulence can cause modal power coupling effects on a Gaussian data beam and significantly degrade the mixing efficiency between the data beam and a Gaussian local oscillator (LO) in the coherent detector. Specifically, for widely used single-mode-fiber (SMF)-coupled coherent detectors, such degradation is mainly caused by the significantly reduced efficiency when coupling the multi-mode data beam into the SMF. Optical phase conjugation (OPC) in a photorefractive crystal can "automatically" mitigate turbulence by (a) recording a back-propagated turbulence-distorted probe beam, and (b) creating a phase-conjugate beam that has the inverse phase distortion of the medium as the transmitted data beam. However, previously reported crystal-based OPC approaches for FSO links have demonstrated either: (1) a relatively fast response time of 35 ms but at a relatively low data rate (e.g., <1 Mbit/s), or (2) a relatively high data rate of 2-Gbit/s but at a slow response time (e.g., >60 s). Here, we report an OPC approach for the automatic mitigation of dynamic turbulence that enables both a high data rate (8 Gbit/s) data beam and a rapid (<5 ms) response time. For a similar data rate, this represents a 10,000-fold faster response time than previous reports, thereby enabling mitigation for dynamic effects. In our approach, the transmitted pre-distorted phase-conjugate data beam is generated by four-wave mixing in a GaAs crystal of three input beams: a turbulence-distorted probe beam, a Gaussian reference beam regenerated from the probe beam, and a Gaussian data beam carrying a high-speed data channel. We experimentally demonstrate our approach in an 8-Gbit/s quadrature-phase-shift-keying coherent FSO link through emulated dynamic turbulence. Our results show an up to ∼10-dB improvement in the free-space-to-SMF coupling efficiency for the data beam under dynamic turbulence with a bandwidth of up to ∼260 Hz (Greenwood frequency). Our approach has the potential to significantly increase the resilience of high-performance coherent FSO links to turbulence.

https://doi.org/10.1364/OPTICA.541823

1. INTRODUCTION

Free-space optical (FSO) communication systems have gained increasing interest in many diverse applications due to the promise of a higher data rate and a lower probability of intercept compared to radio-frequency communications [1–4]. Currently, many FSO link demonstrations use intensity modulation and direct detection (IM/DD) [5]. However, coherent detection with a local oscillator (LO) enables significant and compelling advantages for FSO links, including (a) better receiver sensitivity and (b) higher spectral efficiency when utilizing higher-order modulation formats (e.g., quadrature-phase-shift-keying (QPSK) and quadrature-amplitude-modulation (QAM)) [6–8].

Unfortunately, atmospheric turbulence is a key challenge in coherent FSO links [7,9,10]. In a typical coherent detector, a Gaussian data beam efficiently mixes in the photodiode with an LO that has a similar Gaussian modal structure [6]. However, dynamic turbulence (e.g., at the Greenwood frequency of a few hundreds of hertz [11,12]) can cause wavefront distortion of the transmitted data beam and produce modal power coupling from the transmitted spatial mode (typically, a fundamental Gaussian mode) to many higher-order modes [11,13,14]. Therefore, optoelectronic mixing between the turbulence-distorted multi-mode data beam and a single-Gaussian-mode LO beam becomes significantly degraded in coherent detection (e.g., with a mixing loss >20 dB)

[14,15]. In different system implementations, such loss can result from (1) reduced efficiency when coupling the multi-mode data beam to a single-mode-fiber (SMF) for an SMF-coupled coherent detector [14] or (2) modal mismatch between the multi-mode data beam and the Gaussian LO in a free-space-coupled detector [15]. Various approaches for adaptive dynamic turbulence mitigation in coherent FSO links include (a) adaptive optics by measuring the wavefront distortion and correcting it through an electronic feedback loop [8,16–19] and (b) coherent multi-mode combining by collecting multiple modes and combining them using additional electronic iterative digital signal processing (DSP) [20–22] or a photonic integrated circuit with electronic feedback controls [23–25].

Alternatively, it might be highly advantageous to "automatically" mitigate and adapt to dynamic turbulence without the need for electronic signal processing [26–28]. One approach is to use optical phase conjugation (OPC) based on the photorefractive effects in a crystal [29–34], including the following: (1) a probe beam reverse-propagates from the receiver (Rx) to the transmitter (Tx) and experiences distortion due to turbulence; (2) this probe beam "writes" its turbulence-induced phase distortion into a crystal; (3) a forward-propagating Tx beam "reads" the crystal and takes on the conjugate of the phase distortion (i.e., the inverse effect) of the turbulence-affected probe beam; and (4) this conjugate beam propagates through the same turbulence to the Rx and the turbulence distortion is automatically mitigated [32]. Crystal-based OPC was shown using (1) self-pumped two waves in which the probe beam itself also acts as the read-out beam [32,35–38], and (2) four-wave mixing (FWM) with a separate writing (probe), read-out (data) beam and reference beam [32,39,40]. For the self-pumped scheme, a relatively rapid response time of 35 ms was achieved but at a relatively low <1-Mbit/s data rate (due to the use of a free-space modulator) [36–38,41]. For the FWM-based approach, a relatively high data rate of 2 Gbit/s was achieved (due to the use of a high-speed fiber-coupled modulator), but the response time of >60 s was too slow to mitigate dynamic turbulence effects [32,40].

In this paper, we achieve both high data rates and rapid response times simultaneously. We experimentally demonstrate the automatic mitigation of dynamic turbulence in an 8-Gbit/s QPSK coherent FSO link using FWM-based OPC in an undoped GaAs crystal with a <5 ms response time. We transmit a Gaussian probe beam from the Rx to the Tx through emulated turbulence. At the Tx, we create a Gaussian reference beam from the distorted probe beam through SMF-based mode filtering and an optical amplifier. Moreover, we generate a Gaussian beam carrying an 8-Gbit/s QPSK data signal through an SMF-coupled phase modulator. Subsequently, a phase-conjugate data beam is generated through an FWM process in the crystal with the inputs of the probe, reference, and data beams. When the phase-conjugate beam propagates through turbulence to the Rx, turbulence-induced beam distortion and modal coupling are mitigated, and efficient free-space-to-SMF coupling and coherent heterodyne detection is enabled. Under emulated dynamic turbulence with a Greenwood frequency of ∼260 Hz, our approach shows an up to ∼10-dB improvement in the free-space-to-SMF coupling efficiency. Moreover, our mitigation achieves bit-error ratios (BERs) below the 7% forward error correction (FEC) limit for 400 different dynamic turbulence realizations, while a conventional coherent link has ∼41% of the realizations above the FEC limit. Compared to prior demonstrations of crystal-based OPC turbulence mitigation, we show ∼10,000-fold faster response time for coherent FSO links with an 8 Gbit/shigh-speed data rate through dynamic turbulence.

2. CONCEPT

A. Matrix Representation of Turbulence-induced Modal Coupling for Bidirectional Beam Propagation

Before showing the concept of our approach, we outline the theory of OPC-based turbulence mitigation by utilizing matrix operations to represent turbulence-induced modal coupling. The wavefront of an optical beam can be distorted when propagating through atmospheric turbulence, causing power coupling from the transmitted spatial mode to other modes [11] (e.g., Laguerre–Gaussian ($LG_{\ell,p}$) modes with indices ℓ and p [42]). This modal coupling process can be approximately represented as matrix manipulation [43],

$$\boldsymbol{E}_{\text{out}} = U\boldsymbol{E}_{\text{in}}, \tag{1}$$

where the vectors $\boldsymbol{E}_{\text{in}}$ and $\boldsymbol{E}_{\text{out}}$ describe the complex coefficients of the LG mode components of the input and output optical fields, respectively. Here, we consider a bidirectional beam propagation scenario between a pair of Tx and Rx. Each $\boldsymbol{E}_{\text{in}}$ and $\boldsymbol{E}_{\text{out}}$ vector has $2N$ elements, where the first N elements describe the coefficients of modes at the Tx, and the second N elements describe the modes at the Rx. Here, N corresponds to the number of LG modes that can be transmitted/detected at the Tx/Rx [43]. These N modes can be ranked in the vector by their mode-group orders (i.e., $2p + |\ell|$) [44]. The first element in the vector represents the fundamental Gaussian mode ($LG_{\ell=0,p=0}$). The modal-coupling matrix U with $2N \times 2N$ dimensions can be written as [43]

$$U = \begin{bmatrix} 0 & T_{rt}^{\leftarrow} \\ T_{tr}^{\rightarrow} & 0 \end{bmatrix}, \tag{2}$$

where the $N \times N$ matrix $T_{tr}^{\rightarrow}$ represents the modal coupling for the beam propagating from the Tx to the Rx and the $N \times N$ matrix $T_{rt}^{\leftarrow}$ represents the beam propagating from the Rx to the Tx. If Tx and Rx can capture all the modes reaching them from the other end, the transmission through turbulence can be considered as a unitary process [27,45,46]. Therefore, we have

$$T_{tr}^{\rightarrow \text{H}} T_{tr}^{\rightarrow} = I \text{ and } T_{rt}^{\leftarrow \text{H}} T_{rt}^{\leftarrow} = I, \tag{3}$$

where H denotes the conjugate transpose of a matrix, and I is an ***identity*** matrix. Moreover, due to the reciprocal property of turbulence [47,48], the matrix $T_{tr}^{\rightarrow}$ is the transpose matrix of $T_{rt}^{\leftarrow}$,

$$T_{rt}^{\leftarrow} = T_{tr}^{\rightarrow \text{T}}. \tag{4}$$

Based on Eqs. (3) and (4), we have

$$\begin{aligned} UU^{*} &= \begin{bmatrix} 0 & T_{rt}^{\leftarrow} \\ T_{tr}^{\rightarrow} & 0 \end{bmatrix} \begin{bmatrix} 0 & T_{rt}^{\leftarrow *} \\ T_{tr}^{\rightarrow *} & 0 \end{bmatrix} \\ &= \begin{bmatrix} 0 & T_{tr}^{\rightarrow \text{T}} \\ T_{rt}^{\leftarrow \text{T}} & 0 \end{bmatrix} \begin{bmatrix} 0 & T_{rt}^{\leftarrow *} \\ T_{tr}^{\rightarrow *} & 0 \end{bmatrix} = I. \end{aligned} \tag{5}$$

Equation (5) shows that the matrix multiplication of U and its complex conjugate U^{*} results in an identity matrix, which is a key theoretical foundation that supports the use of phase conjugation for turbulence mitigation.

B. Turbulence Mitigation Using OPC for Coherent FSO Communication Links

As shown in Fig. 1(a), atmospheric turbulence can significantly degrade the performance of a coherent FSO link. At the Tx, a fundamental Gaussian beam (i.e., $LG_{0,0}$ mode) carrying a data signal ($S(t)$) is transmitted through turbulence to the Rx. The turbulence can cause power coupling from the $LG_{0,0}$ mode to many other modes. According to Eqs. (1) and (2), the turbulence-distorted data beam can be represented as

$$\boldsymbol{E}_{d_r} = U\boldsymbol{E}_{d_t} = \begin{bmatrix} 0 & T_{rt}^{\leftarrow} \\ T_{tr}^{\rightarrow} & 0 \end{bmatrix} \begin{bmatrix} \begin{pmatrix} 1 \\ 0 \\ \vdots \\ 0 \end{pmatrix}_{N\times 1} \\ \begin{pmatrix} 0 \\ 0 \\ \vdots \\ 0 \end{pmatrix}_{N\times 1} \end{bmatrix} \cdot S(t), \quad (6)$$

where $\boldsymbol{E}_{d_t}$ and $\boldsymbol{E}_{d_r}$ are mode representations of the optical data beams at the Tx and the Rx, respectively, and $S(t)$ is the modulated data signal. Therefore, the turbulence-distorted beam at the Rx contains many modes, which correspond to the first column of the matrix $T_{tr}^{\rightarrow}$. At the Rx, a Gaussian-mode ($LG_{0,0}$) local oscillator (LO) is utilized to optoelectrically mix with the received data beam to recover the data signal using coherent detection. However, the turbulence-distorted data beam is a multi-mode beam, and only the power on the $LG_{0,0}$ modal component (i.e., the first element of the first column of $T_{tr}^{\rightarrow}$) of the beam efficiently mixes with the LO. Such mixing loss can happen for both (1) a free-space-coupled detector due to the orthogonality between the higher-order modes and the Gaussian LO [15] and (2) an SMF-coupled detector where the higher-order modes at most barely couple into fiber [14,49]. Therefore, coherent detection becomes significantly inefficient, which results in a lower quality of the received data signal. In this paper, we focus on an FSO system with an SMF-coupled coherent detector and address the challenge of turbulence-induced reduction in free-space-to-SMF coupling efficiency.

Figure 1(b) shows the concept of our approach utilizing an OPC to mitigate turbulence in a coherent FSO link. We transmit

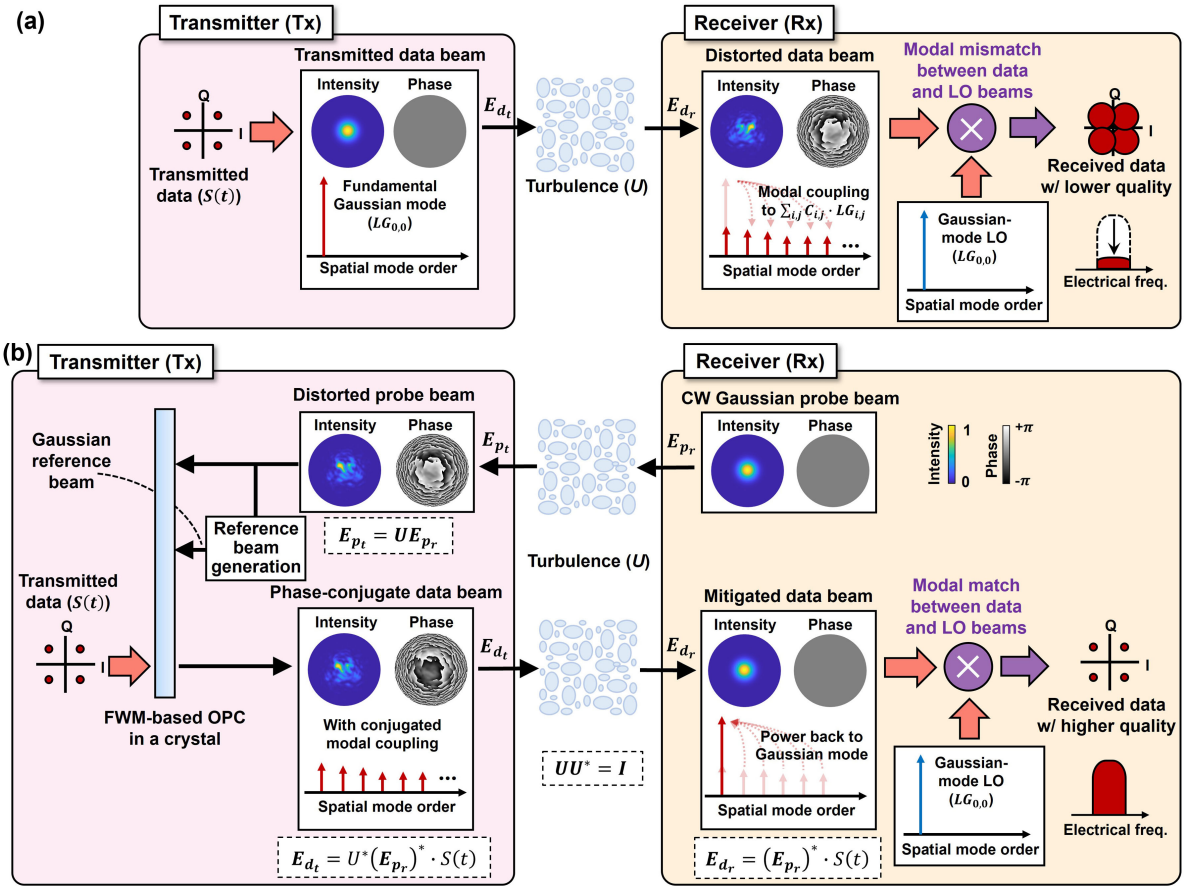

Fig. 1. Concept of utilizing OPC to mitigate turbulence in coherent FSO links. (a) A conventional coherent FSO link can be significantly degraded by turbulence. The transmitted Gaussian-mode ($LG_{0,0}$) data beam ($\boldsymbol{E}_{d_t}$) carrying the data channel ($S(t)$) is distorted by turbulence, and its power is coupled to many other modes ($\sum_{i,j} C_{i,j} \cdot LG_{i,j}$). At the Rx, the mixing between the distorted beam and a Gaussian LO beam becomes significantly inefficient in coherent detection due to the modal mismatch between the two beams, thus resulting in lower quality of the recovered data. (b) Our proposed coherent FSO link uses OPC to mitigate turbulence. A CW Gaussian probe beam ($\boldsymbol{E}_{p_r}$) propagates from the Rx to the Tx and is distorted by turbulence. At the Tx, a phase-conjugate data beam is created by a fast (compared with the turbulence dynamics) FWM-based OPC with the inputs of the distorted probe beam ($\boldsymbol{E}_{p_t} = U\boldsymbol{E}_{p_r}$), a Gaussian reference beam, and a Gaussian data channel ($S(t)$). The phase-conjugate data beam ($\boldsymbol{E}_{d_t} = U^*\boldsymbol{E}_{p_r}^* \cdot S(t)$) is transmitted along the reverse path through the same turbulence to the Rx. Due to the turbulence-induced modal coupling matrix satisfying $UU^* = I$, the data beam ($\boldsymbol{E}_{d_r} = \boldsymbol{E}_{p_r}^* \cdot S(t)$) is recovered to a Gaussian mode and can be efficiently mixed with a Gaussian LO for coherent detection at the Rx.

a continuous-wave (CW) Gaussian-mode probe beam ($\boldsymbol{E}_{p_r}$) from the Rx through turbulence to the Tx,

$$\boldsymbol{E}_{p_t} = U\boldsymbol{E}_{p_r} = \begin{bmatrix} 0 & T_{rt}^{\leftarrow} \\ T_{tr}^{\rightarrow} & 0 \end{bmatrix} \begin{bmatrix} \begin{pmatrix} 0 \\ 0 \\ \vdots \\ 0 \end{pmatrix}_{N\times 1} \\ \begin{pmatrix} 1 \\ 0 \\ \vdots \\ 0 \end{pmatrix}_{N\times 1} \end{bmatrix}. \tag{7}$$

At the Tx, the turbulence-distorted probe beam ($\boldsymbol{E}_{p_t}$) acts as an input to an optical phase conjugator for generating a beam with phase-conjugated spatial distribution. In our approach, an FWM-based OPC process in a crystal is implemented. A data-modulated optical signal ($S(t)$) is created and acts as a Gaussian input beam to the FWM process. Therefore, a phase-conjugate data beam ($\boldsymbol{E}_{d_t}$) is generated at the Tx,

$$\boldsymbol{E}_{d_t} = \left(\boldsymbol{E}_{p_t}\right)^* \cdot S(t) = U^*\left(\boldsymbol{E}_{p_r}\right)^* \cdot S(t). \tag{8}$$

When the phase-conjugate beam propagates back along the same path through the turbulence, the turbulence-induced modal coupling is automatically mitigated,

$$\boldsymbol{E}_{d_r} = U\boldsymbol{E}_{d_t} = UU^*\left(\boldsymbol{E}_{p_r}\right)^* \cdot S(t) = \left(\boldsymbol{E}_{p_r}\right)^* \cdot S(t). \tag{9}$$

The mitigated data beam ($\boldsymbol{E}_{d_r}$) at the Rx becomes the conjugation of the single-Gaussian-mode CW probe beam modulated by the data signal, $(\boldsymbol{E}_{p_r})^* \cdot S(t)$. As a result, the mitigated data beam can be efficiently coupled to an SMF for coherent detection and achieve higher quality of the received data as compared to the case without mitigation. Here, Eq. (9) is ideal if (1) the phase conjugation process is fast enough so that the phase-conjugate data beam propagates through the same turbulence and experiences the same modal coupling (U) as the probe beam and (2) the Tx and Rx apertures can capture all the modes so that the U is a unitary matrix.

C. Implementation of our Phase Conjugation Architecture Based on FWM in a GaAs Crystal

Figure 2 shows a schematic diagram of our architecture of the OPC for turbulence mitigation. A CW Gaussian probe beam is generated by Laser 1 at the Rx and propagates to the Tx through dynamic turbulence. At the Tx, the turbulence-distorted probe beam is divided by a beam splitter into two copies. One copy is first coupled into an SMF, then amplified by an optical amplifier with a constant output power, and then finally coupled out to free space. In this way of spatial-mode filtering, we generate a collimated Gaussian reference beam that has a fixed power and is mutually coherent with the probe beam. The reference beam and the other copy of the distorted probe beam interfere and illuminate the crystal. Here, we use a GaAs semiconductor crystal, which has a fast response time (can be less than 1 ms [50–52]) at near-infrared wavelengths. At the same time, an optical data channel is generated at the Tx by modulating Laser 2 using an SMF-coupled high-bandwidth modulator. This data channel is coupled out to a free-space and collimated Gaussian beam and hits the crystal in a direction opposite to that of the Gaussian reference beam. Through FWM involving the three input beams illuminating the crystal, a phase-conjugate data beam is created and transmitted through the (ideally) same turbulence back to the Rx for coherent detection. The Gaussian LO beam can be created from the same laser source (Laser 1) as the probe beam.

Such an OPC process can also be explained by a holography model [32]. The interference between the mutually coherent Gaussian reference beam and the distorted probe beam produces interference fringes inside the crystal. Given that the refractive-index change of the crystal is proportional to the light intensity, the intensity of interference creates a holographic grating that is "recorded" inside the crystal [32]. The Gaussian data beam acts as a "read" beam and is diffracted by the grating in a reverse direction of the probe beam. The diffracted data beam would process the phase conjugation of the spatial information of the probe beam (please see Supplement 1, Note 1 for additional information).

In a previous paper, we demonstrated a similar OPC architecture but using a photorefractive oxide crystal ($KbNO_3$) [40]. However, this previous implementation faced two significant challenges due to the crystal's extremely slow response time (>60 s):

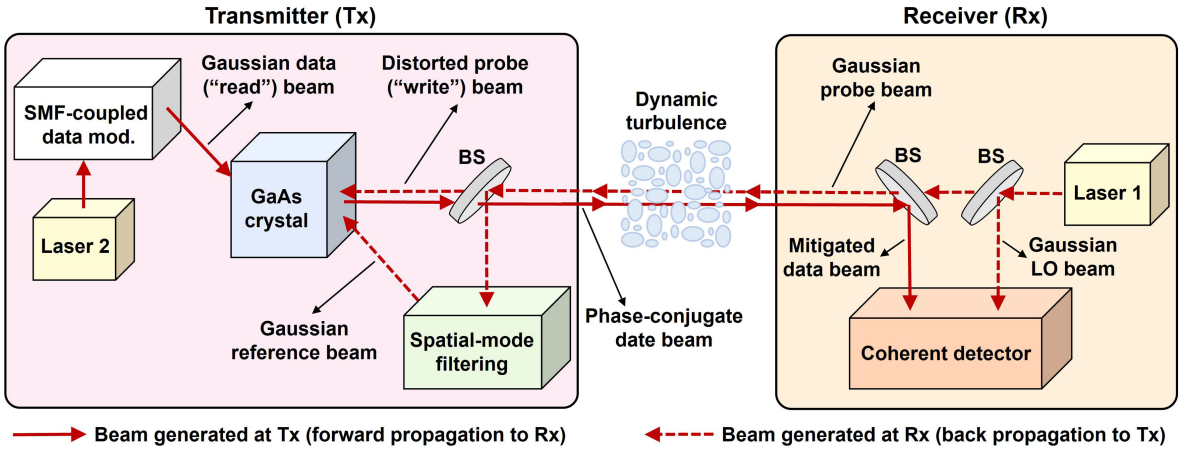

Fig. 2. Our proposed architecture of OPC for turbulence mitigation. The distorted probe beam is split into two copies. One copy is coupled to an SMF and amplified by an optical amplifier to generate a Gaussian reference beam. An optical data channel is generated by an SMF-coupled modulator and coupled to free space to create a Gaussian data beam. Through four-wave mixing (FWM) in a GaAs crystal, a phase-conjugate data beam can be created and transmitted to the Rx along the reverse propagation direction of the probe beam. Mod, modulator; BS, beam splitter; SMF, single-mode fiber.

(1) Mitigating dynamically changing turbulence. Effective "recording" of turbulence distortions required more than 60 seconds of stable illumination and interference of the probe and reference beams in the $KbNO_3$ crystal [40], making it unsuitable for mitigating dynamic turbulence conditions.
(2) Amplifying the reference beam. In general, the power of the reference beam can be boosted to enhance the beam interaction inside the crystal for OPC generation [32]. However, in our previous demonstration, amplifying the reference beam using a fiber-based amplifier was challenging due to the fiber's instability introduced by environmental and temperature variations [53]. This instability can cause phase changes and disrupt the interference between the probe and reference beams, resulting in ineffective turbulence "recording" [40].

In our current work, we instead implement the OPC architecture using a GaAs semiconductor crystal, which can offer a ~ 10,000 times faster response time due to its higher carrier mobility and photosensitivity in the near-infrared range [50]. This faster response time enables our current implementation of the architecture to address the previous challenges, therefore supporting (1) the mitigation of dynamic turbulence, and (2) the use of a fiber amplifier to amplify the reference beam.

3. EXPERIMENTAL SETUP

As a proof-of-concept demonstration, we built the experimental setup, as shown in Fig. 3. More details are provided in the Supplement 1, Note 2. At the Rx, a CW beam is generated by a laser at ~1064 nm, amplified by a ytterbium-doped fiber amplifier (YDFA), and coupled out to free space as a Gaussian probe beam. The probe beam propagates from the Rx to the Tx through dynamic turbulence, which is emulated by a rotating phase screen placed around the middle of a ~1-m free-space link. The phase screen is designed based on Kolmogorov turbulence power spectrum statistics [9]. The Fried parameter r_0 is used to characterize the strength of the emulated turbulence and a smaller r_0 means stronger turbulence [11]. Based on the rotation speed (i.e., round/sec.), we can calculate the Greenwood frequency f_G (see Supplement 1, Note 3 for the calculation), which is commonly used to characterize the rate of turbulence change [11,12]. At the Tx, we use a beam splitter to create two copies of the probe beam, with one being coupled to an SMF and amplified by a YDFA for generating a Gaussian reference beam. Moreover, we create a Gaussian data beam carrying an 8-Gbit/s QPSK signal by modulating a laser through an SMF-coupled phase modulator.

In our experiment, both the collimated Gaussian probe and data beams have a waist diameter of ~2.5 mm. A phase-conjugate data beam is generated by the proposed optical phase conjugator and propagates back toward the Rx through the rotating plate. At the Rx, after being coupled into an SMF, the data beam is mixed with an LO for coherent heterodyne detection. The photoreceiver has a bandwidth of ~10 GHz. After detection, the data signal waveform is captured by a real-time digital sampling oscilloscope with a bandwidth of 20 GHz and a sampling rate of 50 Gsample/s. We measure the complex wavefront of the received data beam using off-axis holography and perform LG modal decomposition to analyze the turbulence-induced modal coupling [14].

4. EXPERIMENTAL RESULTS

A. Modal Coupling Measurements Under Dynamic Turbulence

Figure 4 shows the beam profile and modal-coupling measurements of the received data beam without and with phase

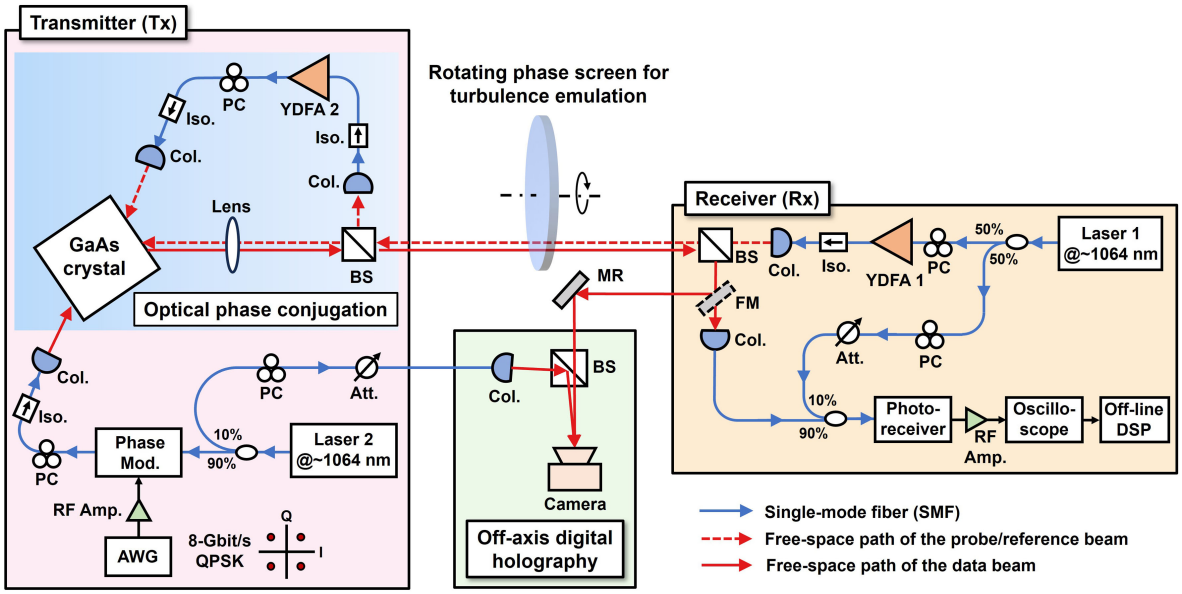

Fig. 3. Experimental setup for turbulence mitigation using OPC in an 8-Gbit/s QPSK coherent FSO link. At the receiver (Rx), a CW Gaussian probe beam is transmitted through emulated dynamic turbulence to the transmitter (Tx). At the Tx, an 8-Gbit/s QPSK data channel is generated through an SMF-coupled phase modulator and coupled to free space as a Gaussian data beam using a laser with no coherence relation to the probe optical source. A phase-conjugate data beam is created by our phase conjugator and propagates back to the Rx through turbulence. At the Rx, for LG spectrum measurement, the data beams are sent to (by a flip mirror, FM) an off-axis holography setup. For the data detection, the data beam is coupled to an SMF and mixed with a Gaussian-mode LO in a photoreceiver. Heterodyne coherent detection is applied, and offline DSP is used to recover the QPSK signal. AWG, arbitrary waveform generator; Mod., modulator; Amp, amplifier; YDFA, ytterbium-doped fiber amplifier; PC, polarization controller; Iso., isolator; Col., collimator; BS, beam splitter; MR, mirror; FM, flip mirror; SMF, single-mode fiber; Att., attenuator; DSP, digital signal processing.

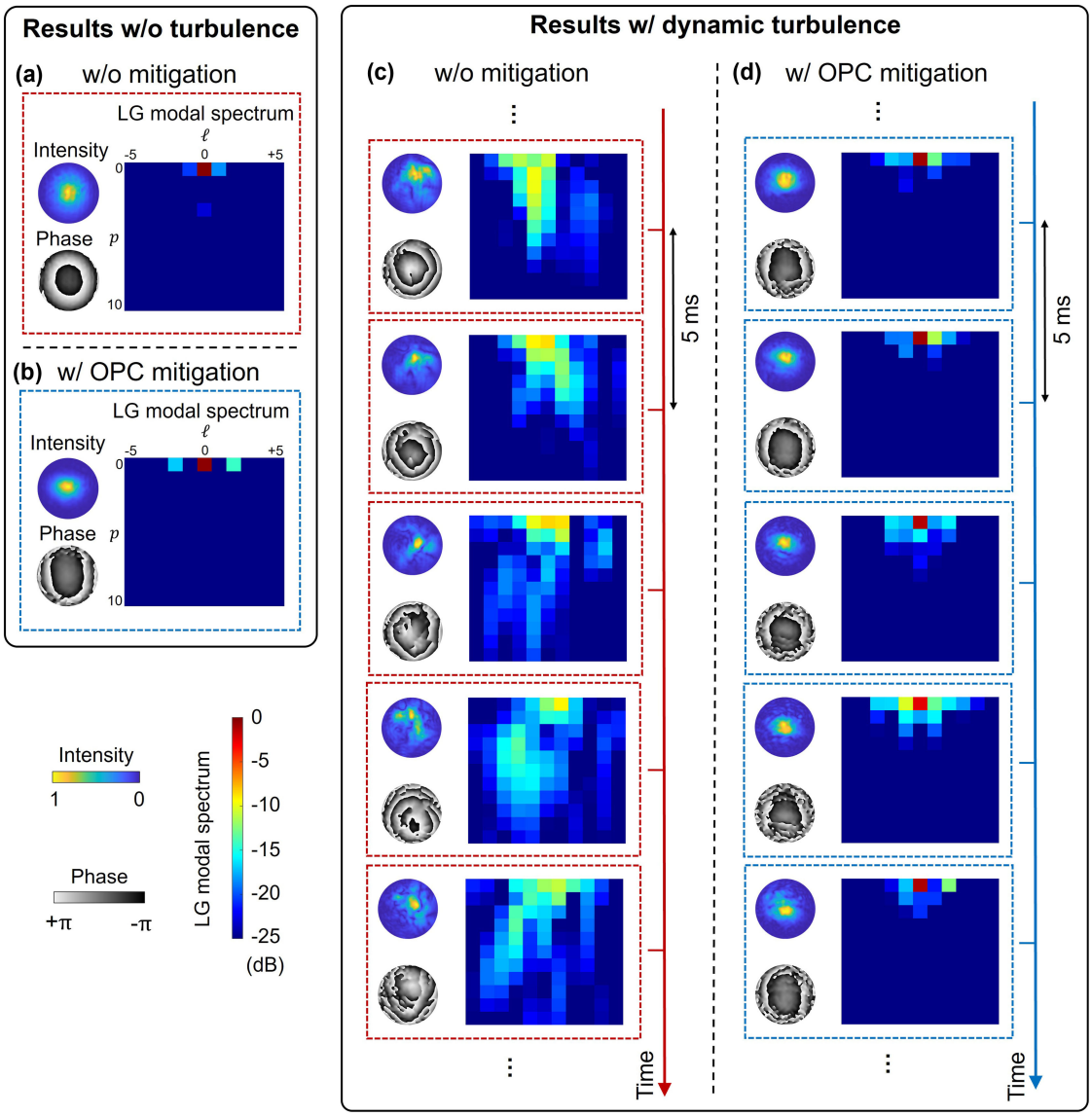

Fig. 4. Experimental results of beam profiles and modal coupling for the received data beam under dynamic turbulence without and with OPC mitigation. Results under no turbulence (a) without mitigation and (b) with mitigation. Results under dynamic turbulence when the turbulence phase screen ($r_0 = 0.6$ mm) is rotating at 2 round/sec (c) without mitigation and (d) with mitigation. For these measurements, we use a camera with a frame rate of 200 frame/s, corresponding to 5 ms per measurement.

conjugation mitigation. For the case without mitigation, we transmit the Gaussian data beam from the Tx to the Rx through the same turbulence phase screen along the same path as the phase-conjugate data beam. As shown in Figs. 4(a) and 4(b), when we remove the turbulence phase screen, most power of the received beam is on the $LG_{0,0}$ mode for both cases of with and without mitigation. Figures 4(c) and 4(d) show the results when the turbulence screen (Fried parameter $r_0 = 0.6$ mm) is rotating at a speed of 2 round/s, which corresponds to a Greenwood frequency f_G of ~260 Hz. Limited by the frame rate (200 frames/sec) of the camera we used, the profile and modal-coupling measurements are taken every 5 ms. Here, we show 5 successive measurements as examples for each case. A movie containing 100 successive frames is provided in the Visualization 1. As shown in Fig. 4(c), the intensity/phase profiles are distorted, and the power of the beam is coupled to multiple modes without mitigation. Both distortion and coupling measures are dynamically changing. With mitigation, the intensity/phase profiles of the received beam can be recovered back to Gaussian-like distribution. Moreover, the power of the beam mostly remains on the $LG_{0,0}$ modal component and only coupled to several neighboring modes, which indicates that our approach can effectively mitigate the turbulence-induced modal coupling within a <5-ms response time.

We also measure turbulence mitigation performance using a faster measurement approach. Specifically, we couple the received beam into an SMF and measured the power using a photodiode with a bandwidth of 10 kHz and a sampling rate of 900 k sample/s. This measurement can help to show the fluctuation of the power remaining on the fundamental Gaussian mode under dynamic turbulence. Figures 5(a)–5(c) also show the results for the case when the turbulence phase screen rotates at a speed of 2 round/s. In Fig. 5(a), we show the power fluctuation measurement over a duration of 4 s and highlight a shorter section of 0.4 s as an example to provide a clearer view of such power fluctuation. We note that

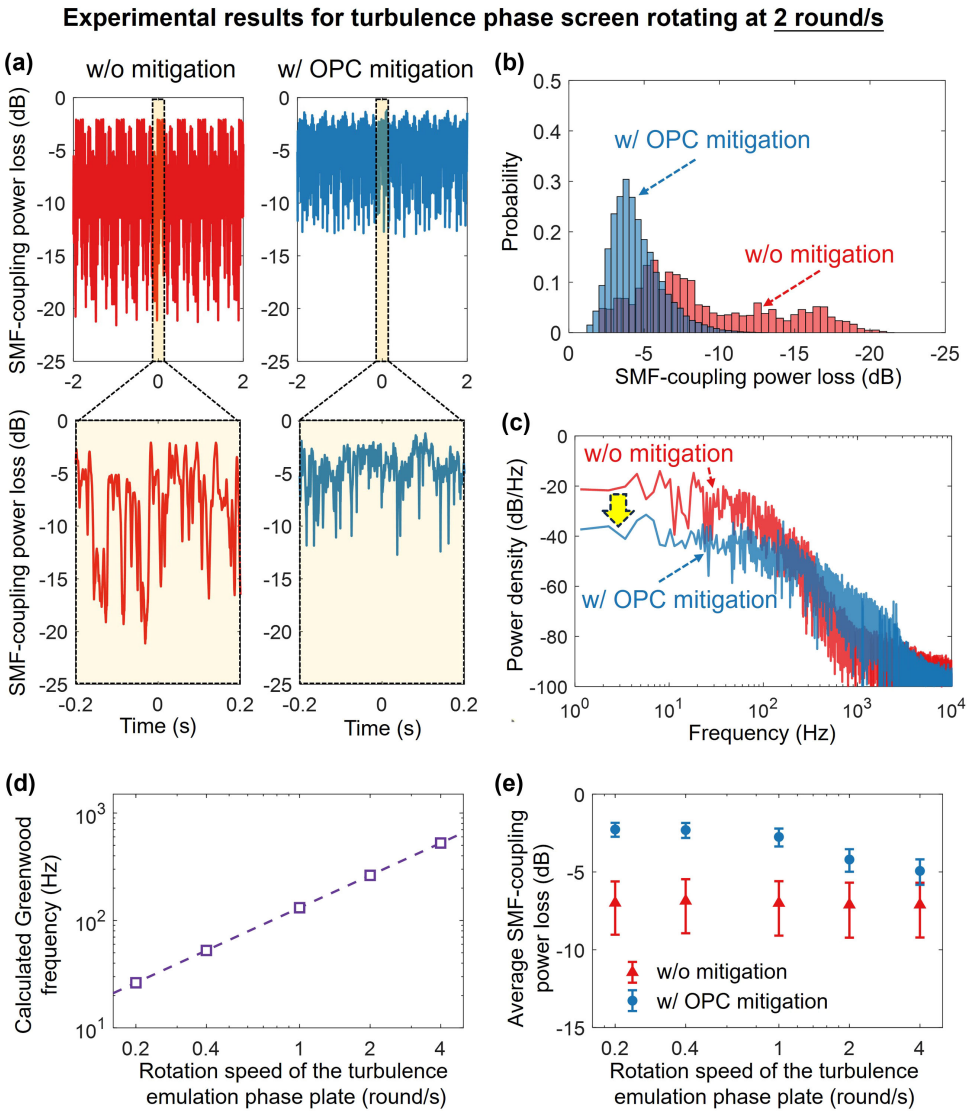

Fig. 5. Experimental results of SMF-coupling power loss of the received data beam under dynamic turbulence. (a) Power fluctuation, (b) probability distribution, and (c) density spectrum of the SMF-coupling loss without and with phase conjugation mitigation. The results in (a–c) are for the turbulence phase screen ($r_0 = 0.6$ mm) rotating at 2 round/sec. The power loss is measured by a fiber-coupled photodiode with a 10 kHz bandwidth at a sampling rate of 900 k sample/sec. (d) Calculated Greenwood frequency for different rotation speeds of the turbulence phase screen. (e) Average SMF-coupling loss for different rotation speeds of the turbulence phase screen. The error bars show the standard deviation of the measurements.

due to the multiple rotation periods of the phase screen within the 4 s interval, the recorded waveform exhibits multiple periodic cycles. We use one cycle period (duration of 0.5 s) of the waveform as an example to calculate the power probability distribution and power spectral density, as shown in Figs. 5(b) and 5(c), respectively. Based on the measured turbulence-induced SMF-coupling loss, our mitigation approach can reduce the power fluctuation range by ∼10 dB. Moreover, we also calculate the power density spectrum in Fig. 5(c). The frequency components below ∼200 Hz are effectively reduced with mitigation, which also indicates that coupled power into the SMF has less fluctuation. In Supplement 1, Note 4, we provide the power fluctuation, probability distribution, and density spectrum of the SMF-coupling loss for other phase screen rotation speeds at 0.2, 0.4, 1, and 4 round/sec. Similar to the results for 2 round/s in Fig. 5, we use one cycle period of the measured waveform to calculate the power probability distribution and power density spectrum for these rotation speeds, except for the case of 0.2 round/s. For the rotation speed of 0.2 round/s, the 4 s measurement does not cover a full cycle period (5 s). Therefore, the entire 4 s measurement is used for the calculation. As calculated in Fig. 5(d), the corresponding Greenwood frequency ranges from ∼25 Hz to ∼500 Hz for different rotation speeds. Figure 5(e) shows the mean and standard deviation of the SMF-coupling loss, both of which are reduced with our OPC mitigation. However, the reduction tends to be lower when the turbulence phase screen is rotating faster. This might be due to a faster rotation of the screen results in a larger amount of higher-frequency turbulence changes [54], and the crystal becomes less efficient for mitigating that higher-frequency components.

We also measure the mean and standard deviation of the SMF-coupling loss under weaker turbulence with a larger $r_0 = 1.8$ mm (see Supplement 1, Note 5). With the same rotation speed of the screen, the screen with a larger r_0 has a smaller Greenwood

frequency f_G [11,55]. The results show that the mean and standard deviation under this turbulence can also be reduced by our approach. We note that the results under dynamic turbulence with and without mitigation are measured at separate times due to the limitations of our measurement setup. Therefore, it is difficult to directly compare the two results for the same time labels.

B. Mitigation of Dynamic Turbulence in an 8-Gbit/s QPSK Coherent FSO Link

Next, we demonstrate the proposed turbulence mitigation in an 8-Gbit/s QPSK FSO communication link. Figure 6 shows the data transmission performance under 400 different turbulence realizations. The results are measured when the turbulence phase screen is continuously rotating at a speed of 2 round/sec, corresponding to the Greenwood frequency of ∼260 Hz (Fried parameter $r_0 = 0.6$ mm). Specifically, we program a code to control the real-time oscilloscope, which sequentially captures and saves 400 waveforms of received data signals. After each waveform is captured, we stop the oscilloscope for a random time period (ranging from 0.5 to 1 s). This pause allows the turbulence phase screen to rotate to a different orientation before capturing the next waveform. As a result, the 400 signal waveforms are highly likely to correspond to different cases of turbulence distortion (i.e., turbulence realizations). However, there remains a low probability that some cases may exhibit similar turbulence distortions. For each turbulence realization, the recorded signal waveform with a duration of 20 μs is used for calculating error vector magnitude (EVM) and BER performance. To focus on the turbulence mitigation performance, we ensure similar optical powers for the transmitted Gaussian (without mitigation) and phase conjugate data beam (with mitigation). Therefore, they have similar performance with EVMs [56] at ∼18% under no turbulence, as shown in Figs. 6(a1) and 6(b1). When there is turbulence, the EVM performance can be degraded up to ∼80% without mitigation, while the EVMs with mitigation are below ∼35% for all realizations. Moreover, our mitigation achieves BER values below the 7% forward error correction (FEC) threshold (BER at 3.8×10^{-3}) [57,58] for all realizations. However, since turbulence can cause strong modal-coupling-induced loss, the performance without mitigation does not achieve the 7% FEC limit for ∼41% of the realizations.

5. DISCUSSION

In this paper, we show turbulence mitigation at a wavelength of ∼1064 nm, dictated by the efficient working wavelength of the GaAs crystal. The data rate and modulation format demonstrated in our experiment are limited by our current modulation equipment at ∼1064 nm. We believe our approach can potentially support higher data rates with more complex formats (e.g., QAM), given that high-performance devices (e.g., I/Q modulator) can be used.

In our OPC architecture, a Gaussian reference beam is regenerated from the turbulence-distorted CW probe beam by SMF coupling and YDFA amplification. We used a high-power YDFA in our experiment having a minimum input optical power of ~ -3 dBm. When the turbulence is stronger, the probe power coupled to the YDFA tends to be weaker and might be lower than the required input power. Therefore, our YDFA might not be able to amplify such weak power for reference beam regeneration. We note that one potential way to handle this issue is using optical injection locking, which can amplify a CW input light with smaller power [59,60].

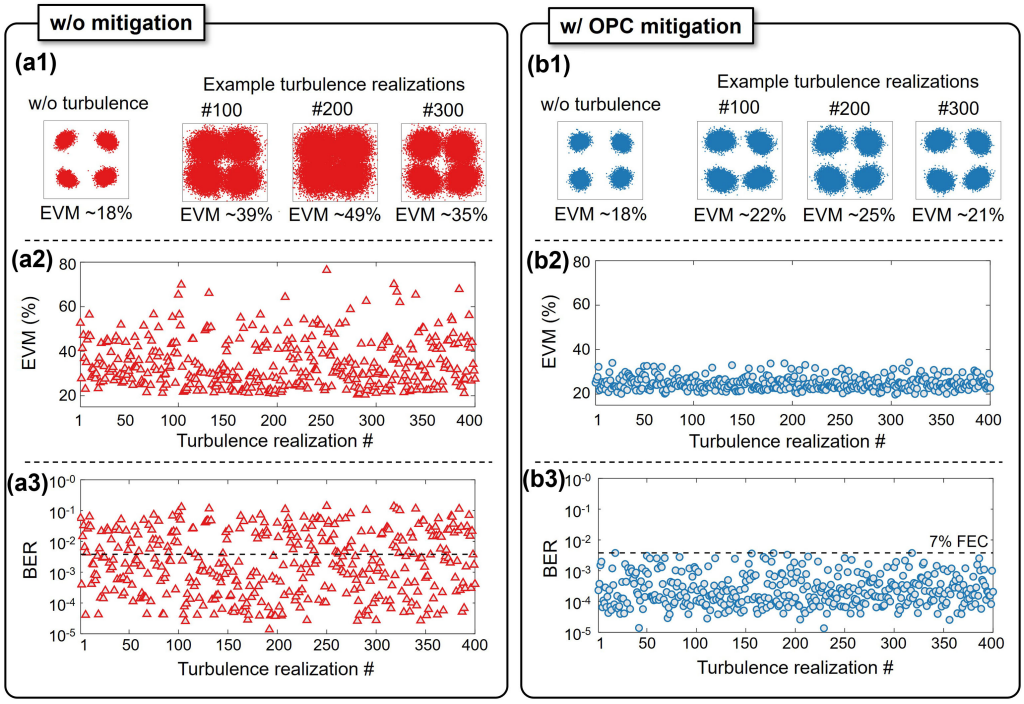

Fig. 6. Experimental results for 8-Gbit/s QPSK data transmission in a coherent FSO link under dynamic turbulence without mitigation and with OPC mitigation. Results are measured for 400 different turbulence realizations when the turbulence phase screen rotates at 2 round/sec., including data constellations in (a1) and (b1), EVM performance in (a2) and (b2), and BER performance in (a3) and (b3). Note that we measure the results with and without mitigation at separate times due to the limitations of our measurement setup. Therefore, the results with the same realization label may correspond to different turbulence realizations and are difficult to be directly compared.

For optical nonlinear processes, power efficiency is always a potential concern. The efficiency in our demonstration for the phase conjugation is roughly 5×10^{-4} (conversion between the Gaussian data beam to the phase-conjugate data beam). While employing the GaAs crystal significantly improves the response time for mitigating dynamic modal coupling induced by turbulence, its efficiency remains low (~ -33 dB), posing a challenge of high power loss during OPC generation. This low efficiency is mainly due to the crystal's small electro-optic coefficient, which results in limited refractive index modulation and low diffraction efficiency of the "recorded" refractive-index grating [61]. However, the efficiency of this crystal can be potentially enhanced through several methods, such as

(1) applying an external electrical voltage across the crystal. An external electric field can increase the charge carrier transport, thereby enhancing the refractive index modulation in the crystal [62]. For instance, previous studies have demonstrated a >500-fold increase in the efficiency of a GaAs crystal by applying an external electric field [62]; and
(2) optimizing the period of the "recorded" grating. Different crossing angles of the probe and reference beams result in different periods of the "recorded" grating [33]. If the grating period is too small or too long, it can disrupt phase matching, weaken nonlinear interactions, and consequently reduce the OPC efficiency [50,62]. The impact of the grating period can be significant (e.g., leading to a >10-fold difference in efficiency [50]) under certain conditions. We believe the crossing angle of the probe and reference beams in the demonstrated architecture can be optimized for a higher OPC efficiency.

The above two points concern the GaAs crystal we used. There is, of course, the possibility that other materials in the future may provide higher efficiency and faster response times [61].

We note that in addition to OPC, other techniques have been previously investigated to "automatically" (e.g., passively) mitigate turbulence [14,26], including (1) a pilot-assisted "self-coherent" FSO system, in which an additional pilot beam is transmitted at the Tx and optoelectronicly mixed with the data beam in a free-space-coupled PD at the Rx [14] and (2) a vector-beam-based FSO link, where data is encoded on turbulence-resilient spatial polarization states (polarization shift keying) of a family of vector beams [26]. However, these techniques were not specifically designed to address turbulence issues for conventional coherent FSO systems.

In Section 2.A, we mentioned that ideal OPC-based turbulence mitigation relies on the Tx aperture capturing all the modal components of the back-propagated probe beam [43]. If this condition is met, then the turbulence-induced modal coupling can be treated as a unitary matrix and can be ideally mitigated by its conjugate counterpart [43]. In general, this condition may not always be satisfied, especially in cases in which a limited-size aperture might truncate and "clip" the received beam. Such issues can be exacerbated due to strong wandering and spreading effects under thick turbulence conditions after long propagation [9]. Due to aperture clipping, not all modal components of the beam would be captured, likely leading to incomplete phase conjugation and degraded turbulence mitigation [63]. Previous studies have investigated such incomplete phase conjugation and have shown that a smaller Tx aperture results in lower fidelity of the OPC-mitigated beam [64]. For our general approach, aperture clipping effects can be mitigated by using an appropriately large crystal to collect a large number of incoming modal components, thus reducing the effects of incomplete phase conjugation. However, increasing the size of the crystal might also impact the OPC efficiency and performance [33]. Therefore, a more comprehensive study of using larger crystals may be beneficial in order to meet the challenges of aperture clipping.

We note that the performance of modal coupling mitigation is not ideal in our experiment, with residual power coupling remaining in some higher-order modes [see Fig. 4(d)]. This can be potentially attributed to several factors, including (1) not all modal components of the turbulence-distorted probe beam are captured and "recorded" by the limited-size crystal, resulting in incomplete phase conjugation and imperfect mitigation of the turbulence distortion [63] and (2) the dynamic rotation of our phase plate can induce vibrations of our setup, which causes beam misalignment inside the crystal, therefore degrading phase conjugation results [32].

Funding. Office of Naval Research (N00014-20-1-2558); Airbus Institute for Engineering Research.

Acknowledgment. This work is supported by the Office of Naval Research through the Multidisciplinary University Research Initiative Program and the Airbus Institute for Engineering Research.

Disclosures. The authors declare no competing interests.

Data availability. Data underlying the results presented in this paper are not publicly available at this time but may be obtained from the authors upon reasonable request.

Supplemental document. See Supplement 1 for supporting content.

REFERENCES

1. M. A. Khalighi and M. Uysal, "Survey on free space optical communication: a communication theory perspective," Commun. Surveys Tuts. **16**, 2231–2258 (2014).
2. A. Trichili, M. A. Cox, B. S. Ooi, *et al.*, "Roadmap to free space optics," J. Opt. Soc. Am. B **37**, A184–A201 (2020).
3. H. Hemmati, ed., *Near-Earth Laser Communications*, 2nd ed. (CRC Press, 2021).
4. A. Biswas, M. Srinivasan, R. Rogalin, *et al.*, "Status of NASA's deep space optical communication technology demonstration," in *IEEE International Conference on Space Optical Systems and Applications (ICSOS)* (IEEE, 2017), pp. 23–27.
5. A. Jahid, M. H. Alsharif, and T. J. Hall, "A contemporary survey on free space optical communication: potentials, technical challenges, recent advances and research direction," J. Netw. Comput. Appl. **200**, 103311 (2022).
6. G. Li, "Recent advances in coherent optical communication," Adv. Opt. Photon. **1**, 279–307 (2009).
7. F. P. Guiomar, M. A. Fernandes, J. L. Nascimento, *et al.*, "Coherent free-space optical communications: opportunities and challenges," J. Lightwave Technol. **40**, 3173–3186 (2022).
8. Y. Horst, B. I. Bitachon, L. Kulmer, *et al.*, "Tbit/s line-rate satellite feeder links enabled by coherent modulation and full-adaptive optics," Light Sci. Appl. **12**, 153 (2023).
9. L. C. Andrews and R. L. Phillips, *Laser Beam Propagation Through Random Media*, 2nd ed. (2005).
10. E. Agrell, M. Karlsson, F. Poletti, *et al.*, "Roadmap on optical communications," J. Opt. **26**, 093001 (2024).
11. M. A. Cox, N. Mphuthi, I. Nape, *et al.*, "Structured light in turbulence," IEEE J. Sel. Top. Quantum Electron. **27**, 1–21 (2021).
12. D. P. Greenwood, "Bandwidth specification for adaptive optics systems," J. Opt. Soc. Am. **67**, 390–393 (1977).
13. R. J. Noll, "Zernike polynomials and atmospheric turbulence*," J. Opt. Soc. Am. **66**, 207–211 (1976).
14. R. Zhang, N. Hu, H. Zhou, *et al.*, "Turbulence-resilient pilot-assisted self-coherent free-space optical communications using automatic optoelectronic mixing of many modes," Nat. Photonics **15**, 743–750 (2021).

15. Y. Ren, A. Dang, L. Liu, *et al.*, "Heterodyne efficiency of a coherent free-space optical communication model through atmospheric turbulence," Appl. Opt. **51**, 7246–7254 (2012).
16. M. Chen, C. Liu, D. Rui, *et al.*, "Experimental results of atmospheric coherent optical communications with adaptive optics," Opt. Commun. **434**, 91–96 (2019).
17. Y. Wang, H. Xu, D. Li, *et al.*, "Performance analysis of an adaptive optics system for free-space optics communication through atmospheric turbulence," Sci. Rep. **8**, 1124 (2018).
18. I. Toselli and S. Gladysz, "Improving system performance by using adaptive optics and aperture averaging for laser communications in oceanic turbulence," Opt. Express **28**, 17347–17361 (2020).
19. I. M. Vellekoop, "Feedback-based wavefront shaping," Opt. Express **23**, 12189–12206 (2015).
20. D. J. Geisler, T. M. Yarnall, M. L. Stevens, *et al.*, "Multi-aperture digital coherent combining for free-space optical communication receivers," Opt. Express **24**, 12661–12671 (2016).
21. N. K. Fontaine, R. Ryf, Y. Zhang, *et al.*, "Digital turbulence compensation of free space optical link with multimode optical amplifier," in *45th European Conference on Optical Communication (ECOC)* (IET, 2019), pp. 1–4.
22. N. Liu, C. Ju, D. Wang, *et al.*, "Multi-aperture coherent digital combining based on complex-valued MIMO 2N × 2 adaptive equalizer for FSO communication," J. Lightwave Technol. **41**, 5983–5990 (2023).
23. L. De Marinis, P. S. Kincaid, Y. Lucas, *et al.*, "A silicon photonic 32-input coherent combiner for turbulence mitigation in free space optics links," arXiv (2024).
24. A. I. Martinez, G. Cavicchioli, S. Seyedinnavadeh, *et al.*, "Self-adaptive integrated photonic receiver for turbulence compensation in free space optical links," Sci. Reports **14**, 20178 (2024).
25. A. Billaud, A. Reeves, A. Orieux, *et al.*, "Turbulence mitigation via multiplane light conversion and coherent optical combination on a 200 m and a 10 km link," in *IEEE International Conference on Space Optical Systems and Applications (ICSOS)* (IEEE, 2022), pp. 85–92.
26. Z. Zhu, M. Janasik, A. Fyffe, *et al.*, "Compensation-free high-dimensional free-space optical communication using turbulence-resilient vector beams," Nat. Commun. **12**, 1666 (2021).
27. A. Klug, C. Peters, and A. Forbes, "Robust structured light in atmospheric turbulence," Adv. Photon. **5**, 016006 (2023).
28. S. Singh, B. Sephton, W. Tavares Buono, *et al.*, "Light correcting light with nonlinear optics," Adv. Photon. **6**, 026003 (2024).
29. D. M. Pepper, "Nonlinear optical phase conjugation," in *Laser Handbook* (1985), pp. 333–485.
30. B. Y. Zel'dovich, N. F. Pilipetsky, and V. V. Shkunov, *Principles of Phase Conjugation*, Springer Series in Optical Sciences (Springer, 1985), Vol. **42**.
31. R. W. Boyd, *Nonlinear Optics*, 4th ed. (Academic, 2019).
32. G. S. He, "Optical phase conjugation: principles, techniques, and applications," Prog. Quantum Electron. **26**, 131–191 (2002).
33. R. A. Fisher, *Optical Phase Conjugation* (Academic, 2012).
34. M. Cronin-Golomb, B. Fischer, J. White, *et al.*, "Theory and applications of four-wave mixing in photorefractive media," IEEE J. Quantum Electron. **20**, 12–30 (1984).
35. J. Feinberg, "Self-pumped, continuous-wave phase conjugator using internal reflection," Opt. Lett. **7**, 486–488 (1982).
36. T. Honda and H. Matsumoto, "Reflection-grating self-pumped phase conjugation with $BaTiO_3$:Co and compensation for air turbulence," J. Opt. Soc. Am. B **11**, 1983–1991 (1994).
37. D. M. Pepper, "Hybrid phase conjugator/modulators using self-pumped 0°-cut and 45°-cut $BaTiO_3$ crystals," Appl. Phys. Lett. **49**, 1001–1003 (1986).
38. C. Medrano, M. Zgonik, P. Bernasconi, *et al.*, "Phase conjugation in optical communication links with photorefractive Fe: $KNbO_3$," Opt. Commun. **128**, 177–184 (1996).
39. A. Brignon, J.-P. Huignard, M. H. Garrett, *et al.*, "Spatial beam cleanup of a Nd: YAG laser operating at 1.06 μm with two-wave mixing in Rh: $BaTiO_3$," Appl. Opt. **36**, 7788–7793 (1997).
40. H. Zhou, Y. Duan, H. Song, *et al.*, "Automatic turbulence mitigation for coherent free-space optical links using crystal-based phase conjugation and fiber-coupled data modulation," Opt. Lett. **48**, 2194–2197 (2023).
41. D. M. Pepper, D. A. Rockwell, and G. J. Dunning, "Nonlinear optic phase conjugation," IEEE Circuits Devices Mag. **7**, 21–34 (1991).
42. A. Forbes, M. de Oliveira, and M. R. Dennis, "Structured light," Nat. Photonics **15**, 253–262 (2021).
43. H. Cao, A. P. Mosk, and S. Rotter, "Shaping the propagation of light in complex media," Nat. Phys. **18**, 994–1007 (2022).
44. N. K. Fontaine, R. Ryf, H. Chen, *et al.*, "Laguerre-Gaussian mode sorter," Nat. Commun. **10**, 1865 (2019).
45. I. Nape, K. Singh, A. Klug, *et al.*, "Revealing the invariance of vectorial structured light in complex media," Nat. Photonics **16**, 538–546 (2022).
46. Y. Baek, H. B. De Aguiar, and S. Gigan, "Phase conjugation with spatially incoherent light in complex media," Nat. Photonics **17**, 1114–1119 (2023).
47. J. H. Shapiro, "Reciprocity of the turbulent atmosphere," J. Opt. Soc. Am. **61**, 492–495 (1971).
48. Y. Ren, G. Xie, H. Huang, *et al.*, "Adaptive-optics-based simultaneous pre-and post-turbulence compensation of multiple orbital-angular-momentum beams in a bidirectional free-space optical link," Optica **1**, 376–382 (2014).
49. Y. Dikmelik and F. M. Davidson, "Fiber-coupling efficiency for free-space optical communication through atmospheric turbulence," Appl. Opt. **44**, 4946–4952 (2005).
50. B. Imbert, H. Rajbenbach, S. Mallick, *et al.*, "High photorefractive gain in two-beam coupling with moving fringes in GaAs:Cr crystals," Opt. Lett. **13**, 327–329 (1988).
51. Z. Cheng, C. Li, A. Khadria, *et al.*, "High-gain and high-speed wavefront shaping through scattering media," Nat. Photonics **17**, 299–305 (2023).
52. S. I. Stepanov, V. I. Vlad, D. Popa, *et al.*, "Measuring vibration amplitudes in the picometer range using moving light gratings in photoconductive GaAs:Cr," Opt. Lett. **15**, 1239–1241 (1990).
53. Y. He, K. G. Baldwin, B. J. Orr, *et al.*, "Long-distance telecom-fiber transfer of a radio-frequency reference for radio astronomy," Optica **5**, 138–146 (2018).
54. L. Yang, K. Yao, J. Wang, *et al.*, "Performance analysis of 349-element adaptive optics unit for a coherent free space optical communication system," Sci. Rep. **9**, 13150 (2019).
55. J. H. Lee, S. Shin, G. N. Park, *et al.*, "Atmospheric turbulence simulator for adaptive optics evaluation on an optical test bench," Curr. Opt. Photon. **1**, 107–112 (2017).
56. R. Schmogrow, B. Nebendahl, M. Winter, *et al.*, "Error vector magnitude as a performance measure for advanced modulation formats," IEEE Photon. Technol. Lett. **24**, 61–63 (2012).
57. J. Cho, C. Xie, and P. J. Winzer, "Analysis of soft-decision FEC on non-AWGN channels," Opt. Express **20**, 7915–7928 (2012).
58. B. J. Puttnam, R. S. Luís, E. Agrell, *et al.*, "High capacity transmission systems using homogeneous multi-core fibers," J. Lightwave Technol. **35**, 1157–1167 (2017).
59. R. Kakarla, J. Schröder, and P. A. Andrekson, "One photon-per-bit receiver using near-noiseless phase-sensitive amplification," Light Sci. Appl. **9**, 153 (2020).
60. Z. Su, D. Cai, H. Jiang, *et al.*, "Optical injection locking based local oscillator regeneration for continuous variable quantum key distribution," Opt. Lett. **47**, 1287–1290 (2022).
61. D. D. Nolte, *Photorefractive Effects and Materials* (Springer, 2013).
62. M. Klein, S. McCahon, T. Boggess, *et al.*, "High-accuracy, high-reflectivity phase conjugation at 1.06 μm by four-wave mixing in photorefractive gallium arsenide," J. Opt. Soc. Am. B **5**, 2467–2472 (1988).
63. K. Ridley and E. Jakeman, "Incomplete phase conjugation through a random phase screen. II. Numerical simulations," J. Opt. Soc. Am. A **13**, 2393–2402 (1996).
64. D. Jones and K. Ridley, "Experimental investigation by stimulated Brillouin scattering of incomplete phase conjugation," J. Opt. Soc. Am. B **14**, 2657–2663 (1997).